`

Erosion of Aluminum-Silicon Eutectic Alloy Under Compression Plasma Flows Impact

V.I. Shymanski[a,*](HTTPS://ORCID.ORG/0000-0003-2956-3328), *N.N. Cherenda*[a,**] (HTTPS://ORCID.ORG/0000-0002-2394-5117), *N.V. Bibik*[a,***], *V.M. Astashinski*[b,****](HTTPS://ORCID.ORG/0000-0001-5297-602X), *A.M. Kuzmitski*[b,*****]

[a] *Belarussian State University, Minsk, 220030 Belarus*

[b] *A.V. Luikov Heat and Mass Transfer Institute of the NAS of Belarus, Minsk, 220072 Belarus*

**e-mail: shymanskiv@mail.ru*

***e-mail: cherenda@bsu.by*

****e-mail: bibiknv@bsu.by*

*****e-mail: ast@hmti.ac.by*

****** e-mail: antey@hmti.ac.by*

Abstract— The main physical processes occurring during the impact of compression plasma flows with the eutectic silumin surface were investigated. Numerical modeling of heat transfer processes from the shock-compressed layer formed at the surface of the processed sample by the plasma flow was carried out. It was revealed that the plasma impact leads to melting of the near-surface layer and subsequent crystallization, as a result of which a modified layer was formed. The thickness of melted layer was estimated analytically by solving the classical heat conductivity equation. The experimental depth of the melted layer was also determined using scanning electron microscopy by studying samples cross sections. It was found that the calculated values of the melted layer depth exceeded the experimental ones. This effect was explained by the surface erosion during plasma impact with the material. The main erosion mechanisms were discussed. It was found that hydrodynamic movement of the melt was the main mechanism of surface erosion under compression plasma impact on eutectic silumin. A model was proposed to estimate mass loss during plasma treatment. Good agreement between the experimental and calculated data was obtained.

Keywords: silumin alloy, compression plasma flows, temperature distribution, shock-compressed layer, hydrodynamic flow of melt, erosion, melt velocities, surface wave.

INTRODUCTION

Aluminum-silicon (silumin) alloys are the main piston group materials, which are used to manufacture pistons for internal combustion engines [1-3]. The addition of silicon to aluminum improves its strength properties and wear resistance when operating under high mechanical loads.

`

However, due to the low solubility of silicon in the liquid and solid phases of aluminum, the formation of silumin alloys is accompanied by the crystallization of silicon large inclusions which negatively affect the mechanical properties of the alloy. In addition, silumin alloys of the piston group are alloyed with additional elements in order to increase the heat resistance of these alloys [4-7]. The concentration of the introduced alloying elements is usually limited to fractions or units of percent. Exceeding of these elements solubility limit in aluminum resulted in the formation of brittle coarse intermetallic inclusions leading to ductility loss.

Since the main thermal cycling and mechanical loads on the parts are applied directly to the near-surface layer, the methods of surface modification of the structure and phase state have found wide application. Such methods include pulsed action of high-intensity electron or ion beams, as well as pulsed plasma treatment [8-12]. The feature of such methods of surface modification is the achievement of high temperatures exceeding the melting point in relatively short times comparable with the pulse duration, which allows quenching of the surface layer at the cooling stage, accompanied by directional crystallization. Dispersion of grains and insoluble inclusions, as well as an increase in the solubility limit of the alloy components in each other due to the high crystallization rate are main results of high cooling speed. A number of recent studies have shown the advantage of compression plasma flows (CPF) generated by magnetoplasma compressor for the treatment of silumin alloys of various compositions [10-13]. A special features of such plasma treatment are comparatively high pulse duration (tens to hundreds of microseconds) and high values of energy absorbed by the surface layer of the material resulting in an increase of the melt lifetime and initiation of a number of liquid-phase processes in the molten surface layer. Due to the processes of alloy components mixing in a liquid state homogenization of the elemental composition is occurred resulting in the absence of large inclusions of silicon (as well as other phases) after surface layer crystallization. The thickness of the modified layers reaches 50 μm, which is quite sufficient from the point of view of practical use of materials.

However, the high duration of the plasma pulse, which helps to increase the time of the surface layer of the processed material at elevated temperatures in the molten state, lead also to the growth of surface erosion intensity and sample mass decrease after each plasma pulse. The decrease in mass is directly related to the change in the linear dimensions of the sample, in particular, its thickness, which must be taken into account when processing parts, the dimensional accuracy of which is a prerequisite for their reliable operation. In addition, the removal of a thin surface layer due to erosion processes directly affects the implementation of a combined method for modifying the surface of materials, in which a metal coating is deposited before plasma exposure [10, 12]. The material of such a coating serves as an alloying element for the base alloy, and the alloying process itself occurs in the mode of molten layers mixing. Due to the introduction of alloying elements in this way, it is possible to form additional strengthening phases and ensure the formation of metastable supersaturated solid solutions that have a positive effect on the mechanical properties of the modified layer. Erosion processes leading to the removal of a thin surface layer can significantly change the ratio of the alloying element and the base alloy and make such a combined method, in principle, unsuitable for improving the physical and mechanical properties of the material being processed.

Thus, the analysis of erosion processes of materials surface processed by pulsed high-intensity action is a relevant and important task. The development of a physical-mathematical model of eutectic

`

silumin surface erosion during compression plasma flows impact in the melting mode, taking into account the hydrodynamic movement of the melt, and model verification based on comparison with experimental data were the aims of this work.

EXPERIMENTAL

Piston silumin alloy of eutectic composition (11.0-13.0 Si, 0.8-1.5 Cu, 0.8-1.3 Mg, 0.2 Zn, 0.2 Mn, 0.2 Ti, 0.8-1.3 Ni, balance Al, in wt.%) was investigation object. Samples have cylindrical shape with a diameter of 15 mm and a thickness of 5 mm. The surface of the samples was treated by three pulses of compression plasma flows (CPF). Plasma flows generation was carried out in a residual nitrogen atmosphere (pressure of 400 Pa) by magnetoplasma compressor of a compact geometry [13]. The forming intrinsic magnetic field ensured compression of the accelerated plasma flow and formation of a compression region in the center of the flow with a diameter of 2 - 3 cm. The diameter of the plasma flow exceeded the diameter of the samples used, which made it possible to achieve a uniform effect of plasma on the entire surface of the sample. The duration of one plasma pulse was 100 μs. The location of the processed samples at distances of 10 - 16 cm from the cathode cut led to a change in the energy density, which was absorbed by the surface layer. The value of the density of the absorbed heat flux energy (Q) at a voltage of 4.0 kV on the capacitor system of the discharge device varied from 10 to 35 J/cm^2 per pulse according to calorimetric studies [14]. During plasma interaction with a target surface, only part of plasma flow energy is transformed to thermal energy leading to sample heating. Some part of energy flow also spent on the processes of evaporation, elastic-mechanical action, etc. However, from the point of view of the structural-phase transformations that occur after the end of the plasma pulse and affect the properties of the material being processed, the heat flux is the most important part of the energy transferred.

Amount of mass removed from the samples after plasma treatment was determined using Radwag AS/60/220/C/2/N analytical scale with measurement accuracy of ±0.05 mg.

The surface morphology analysis of the treated samples was carried out using scanning electron microscopy (SEM) on a LEO1455 VP microscope at an accelerating voltage of 20 kV.

RESULTS AND DISCUSSION

Decrease of the metal target mass is one of the effects occurred during the action of compression plasma flows with a target surface which is confirmed by experimental data. Evaporation of atoms from the free surface due to its high temperature is the evident reason for the sample mass reduction. This mechanism can be especially evident in the case when the density of the absorbed energy ensures heating of the surface to a temperature close to the boiling point of the material. However, experimental data indicate an insignificant contribution of evaporation to the total value of the removed mass [15]. Thus another prevailing mechanism for mass removal should be taken into account. Hydrodynamic movement of the melt due to which the material is carried beyond the boundaries of the sample can be the main mechanism of mass removal [16]. Hydrodynamic movement is realized exclusively in the case when the absorbed energy allows to reach the material melting point.

`

One can use the solution of the classical heat conductivity equation without taking into account the internal heat source to evaluate the temperature fields in the surface layer of a silumin alloy during plasma treatment:

$$c\rho\frac{\partial T}{\partial t}=\kappa\frac{\partial^2 T}{\partial x^2}, \quad (1)$$

where c, ρ, κ are the heat capacity, density and thermal conductivity of the material, respectively. This equation is written in one-dimensional form, where the x coordinate is the depth measured from the free surface of the processed sample. Taking into account that the size of the samples used in diameter did not exceed the diameter of the plasma flow, the temperature distribution along the radial directions can be neglected.

Equation (1) was supplemented with the following initial condition to obtain an unambiguous solution:

$$T(x)\big|_{t=0}=T_0, \quad (2)$$

where T_0 is the initial temperature of the entire sample (assumed to be equal to room temperature). Since pulsed heating by a plasma flow allows achieving significant temperature changes only in a thin surface layer, one can assume that the temperature on the back side of the sample ($x=d$) was not changed during the exposure process:

$$T(t)\big|_{x=d}=T_0. \quad (3)$$

The following boundary condition was used on the front surface of the sample to take into account the heat flux leading to the heating of the surface layer:

$$\left.\frac{\partial T}{\partial x}\right|_{x=0}=-\frac{1}{\kappa}\frac{Q}{\tau}, \quad (4)$$

where Q is the density of absorbed energy, τ is the pulse duration.

It should be taken into account that under the action of a plasma pulse, the density of the absorbed energy is a function of time, which is associated with a change in the discharge current in the discharge device of the magnetoplasma compressor. In the calculations, a constant value of the density of the absorbed power was assumed for a duration of τ =100 μs.

Also, to estimate the temperature in the target after plasma exposure, it is necessary to take into account the occurrence of first-order phase transitions, such as melting and crystallization, which require a certain amount of energy. Accounting of the phase transition latent heat was carried out according to the method described in [17]. It is believed that as the temperature approaches the melting point, an increasing portion of the thermal energy is spent not on heating, but on breaking chemical bonds in the crystal lattice, i.e. the thermal energy entering the system does not provide its heating. This can be interpreted as a sharp increase in the heat capacity of the entire system, which was taken into account in the following form:

$$c=c_0+\frac{L}{\sqrt{2\pi}\Delta}\exp\left(-\frac{\left(T-T_m\right)^2}{2\Delta^2}\right), \quad (5)$$

where L is the latent heat of the phase transition, T_m is the melting temperature, Δ is the width of the temperature range over which the latent heat function of the phase transition operates (in the

`

calculations, Δ was chosen to be ±4 °C), c_0 is the heat capacity of the material without phase transition.

The temporal evolution of the surface temperature is shown in Figure 1a. The results show that the maximum surface temperature is reached at the end of the plasma pulse, after which it decreases due to the absence of an external heat source and thermal conductivity to the volume of the unmelted part. Figure 1b shows the results of calculations of the spatial temperature distribution over the depth of the silumin alloy, which is achieved at the end of the plasma pulse. The melting of the surface layer of eutectic silumin begins at an absorbed energy density of 10 J/cm^2, which corresponds to an absorbed power density of 10^9 W/m^2. With the growth of the absorbed energy density, the surface temperature increases, as well as the depth of the layer in which the temperature exceeds the melting point of silumin. At an energy density of 50 - 55 J/cm^2, the surface temperature reaches the boiling point, which makes further increase in energy inappropriate from the point of view of surface properties modification. The depth at which the melting temperature of the material is reached will be considered the thickness of the molten layer.

Figure 2 shows the SEM images of the cross sections of the samples after plasma impact. According to the experimental data CPF impact with 10 J/cm^2 leads to surface melting. An increase in the absorbed energy density resulted in an increase of the melted layer depth. The depth of the melted layer obtained as a result of calculations corresponds to the experimental depth for the samples processed at a small Q value and exceeds the experimental one for the samples processed at large Q values in the studied energy range (Table). At the maximum value of Q = 35 J/cm^2, the depth obtained in the simulation is equal to 65 μm, while according to the experimental data it is only 45 μm. This is explained by the fact that the plasma impact on silumin is accompanied by the process of erosion of the processed near-surface layer, which entails a decrease in the thickness of the modified layer.

To analyze the hydrodynamic spreading of the melt, it is necessary to consider the interaction of the plasma flow with the target surface. At the initial stage of interaction, there is a rapid transfer of energy to a thin surface layer, as a result of which it passes into a gas-plasma state due to evaporation and ablation. The incident plasma flow does not allow this layer to dissipate into the surrounding space and holds it near the target surface. The formation of such a layer, called a shock-compressed layer, has been repeatedly discussed in the literature [18]. The shock-compressed layer serves as a barrier layer through which thermal energy is transferred from the plasma flow to the material due to thermal conductivity and radiation, which allows us to formulate the boundary condition of the thermal conductivity problem in the form of (4). Shock-compressed layer expands due to an increase in its temperature and growth of evaporated atoms density and, hence, its internal pressure (Fig. 3a). The speed with which the expansion occurs is transmitted directly to the surface layer of the target melt, setting it in motion in the radial direction (Fig. 3b).

During the entire pulse of interaction of the plasma flow with the surface of the silumin alloy, the momentum is transferred from the surface layer to the underlying layers due to the forces of viscous friction. The result of such a momentum transfer is a certain spatial distribution of velocities by the depth of the molten layer. It can be assumed that all layers of liquid begin to move from the center of the sample (for the case of a central incidence of the plasma flow on the surface of the sample) in the radial direction parallel to each other. Neglecting the effect of mixing of individual

`

layers of liquid with each other, it is possible to determine the profile of the melt velocities by depth (Fig. 4), which obeys the Navier-Stokes equation.

The Navier-Stokes equation in a rectangular coordinate system can be written in the following form by choosing the velocity components along the plane and one of them perpendicular:

$$\frac{\partial \vec{v}}{\partial t} + (\vec{v} \cdot \nabla)\vec{v} = -\frac{1}{\rho}\nabla p + \nu \Delta \vec{v}\ , (6)$$

where ν is the kinematic viscosity of the melt, v is the velocity of the melt, ρ is the melt density.

Since only the horizontal component of the velocity is of interest, for the corresponding projection the written equation can be represented in the following form:

$$\frac{\partial v_x}{\partial t} + v_x \frac{\partial v_x}{\partial x} + v_y \frac{\partial v_x}{\partial y} + v_z \frac{\partial v_x}{\partial z} = -\frac{1}{\rho}\nabla p + \nu \left(\frac{\partial^2 v_x}{\partial x^2} + \frac{\partial^2 v_x}{\partial y^2} + \frac{\partial^2 v_x}{\partial z^2} \right). (7)$$

Similar equation can be written for the second component of the velocity v_y.

Assuming that the velocity components v_x and v_y are independent of the horizontal coordinates x and y, and also adopting the approximation of an incompressible melt in which the pressure at all points is the same, the Navier-Stokes equation for the velocity component v_x can be rewritten as:

$$\frac{\partial v_x}{\partial t} = \nu \frac{\partial^2 v_x}{\partial x^2}\ . (8)$$

Here it is also taken into account that the component of the melt velocity v_z is equal to zero, since the main source of the melt motion is the tangential expansion of the shock-compressed layer to its surface. In reality, the shock-compressed layer will also exert pressure on the melt, causing the formation of the velocity component v_z, however, given the small compressibility coefficient of the liquid melt, this component of the velocity can be neglected.

The boundary conditions for the resulting equation are formulated in such a way that at the boundary of the melt and the solid substrate the melt velocity is zero, and at the surface of the molten layer a constant velocity is constantly maintained due to the expansion of the shock-compressed layer. Under such conditions, the solution of the equation (8) can be represented as:

$$v_x(z,t) = v_{0x} erf\left(1 - \frac{z}{2\sqrt{\nu t}}\right), (9)$$

where v_{0x} is the component of the melt velocity directly on the surface.

The obtained solution demonstrates the dependence of the horizontal component of the melt velocity on the depth z and time t. To determine the expansion rate of the shock-compressed layer, as well as the surface flow rate, one can use the laws of formation of surface waves arising as a result of the action of hydrodynamic instabilities, which are described in detail in [19]. The dispersion relation for surface waves has the following form:

$$\omega = \sqrt{kg + \frac{\sigma k^3}{\rho}}\ , (10)$$

where ω is the oscillation frequency of the surface wave, k is the wave number, g is the acceleration due to gravity, σ is the coefficient of surface tension, ρ is the density of the liquid. The first term in expression (10) describes gravitational waves, the second term describes capillary waves. If the

`

thickness of the liquid layer greatly exceeds the length of the surface waves, then the gravitational term can be neglected in the dispersion expression and only the capillary effect of wave generation can be considered. Considering that the oscillation frequency is related to the phase velocity of wave propagation v by the relation $\omega = vk$, we can obtain a relationship between the velocity of the surface wave and its length λ:

$$v = \sqrt{\frac{2\pi\sigma}{\rho\lambda}} . \quad (11)$$

Equation (11) gives the speed at which the layer of liquid melt moves directly on the surface of the sample.

Over time, the surface waves will attenuate due to the dissipation of energy to overcome the viscous friction forces between the layers. However, due to the high cooling rate of the melt, the waves do not have time to attenuate, and the corresponding surface relief form remains after the solidification of the surface layer has. Using the scanning electron microscopy it is possible to determine the characteristic lengths of the surface waves (Figure 4).

Let us assume that the expansion of the shock-compressed layer occurs stationary during the entire existence of the melt. So velocity of the melt surface will be constant. Knowing the distribution of the melt velocity in the radial direction from the center of the sample, we can estimate the mass (volume) of the molten layer that is removed from the sample (Figure 5). Over an infinitely small time interval *dt*, that part of the small sector that is at a distance *vdt* from its edge will be able to leave the sample. The sections of the sector located closer to the center will have time to come closer to the edge of the sample, but will not be able to leave its limits. It is this part of the sector that is whitened in color in the figure.

The elementary mass *dm* removed per unit time *dt* from the sample is related to the melt density ρ and the elementary volume *dV* as follows:

$$dm = \rho dV , \quad (12)$$

Here, the elementary volume *dV* is understood as a thin layer of thickness *dz*, within which the velocity of melt can be considered constant.

Since the melt velocity decreases with depth, the length of the removed sector will also decrease with melt depth. Then the entire mass removed from the surface layer of the sample can be calculated by integration:

$$m = \int dm = 2\pi\rho R \iint v(z,t) dz dt , \quad (13)$$

where *R* is the sample radius.

After substituting the obtained speed value one can obtain:

$$m = 2\pi\rho R v' \int_0^H \int_{T_1}^{T_2} \left(1 - erf \frac{z}{2\sqrt{vt}}\right) dt dz . \quad (14)$$

Here the integration is performed over two independent variables: time and melt depth. The limits of integration over melt depth are determined by the depth of the molten layer *H*. The time integration interval is determined by the start time T_1 and the end time T_2 of the melt existence, which can be determined from the solution of the heat conductivity equation (Figure 6) for different values of the absorbed energy density.

`

Taking into account the initial velocity on the surface of the melt the final expression for removed mass can be written in the following form:

$$m = 2\pi\rho R\sqrt{\frac{2\pi\sigma}{\rho\lambda}}\int_0^H\int_{T_1}^{T_2}\left(1-erf\,\frac{z}{2\sqrt{\nu t}}\right)dtdz\ . \quad (15)$$

A distinctive feature of the obtained solution is its dependence on the sample size (its radius *R*). Indeed, in the case of a sufficiently small sample size, melt droplets torn off from the sample surface will be carried away beyond its limits, thereby reducing its mass. In the case of a large sample diameter, liquid melt droplets carried away will settle on the surface in some proximity to the molten part. Therefore, in the second case, the study of surface erosion due to hydrodynamic processes is difficult from the point of view of sample mass measurement.

The obtained expression allows us to estimate the change of the sample mass during one pulse of the plasma flow action due to hydrodynamic expansion. Using the parameters of the liquid molten silumin of the eutectic composition [20]: density of 2400 kg/m^3, surface tension coefficient of 0.908 N/m and kinematic viscosity of 5.2*10^{-7} m^2/s, and also taking into account different values of the melt existence time and the depth of the molten layer, the dependence of the removed mass values on the value of the absorbed energy density was obtained for a cylindrical sample with a radius of 7.5 mm. The results are shown in Figure 6. The values of the removed mass obtained experimentally and theoretically are of the same order of magnitude, but there is significant discrepancy in the values of the removed mass exist. The reason for such discrepancy is the part of the melt that left the surface, but remained at the lateral side of the sample as a result of the action of surface tension forces. This part of the melt increases the radius of the sample in its upper part (Fig. 7). By measuring the radius of the sample in the upper part and height of this part one can estimate the mass of the melt that reached the edge of the sample but remained on its lateral side. Addition of this mass value to the experimentally determined value of mass removed from the surface (corrected experimental data set in Fig. 6) gives good agreement with the calculated data.

The proposed description of surface erosion can be used at absorbed energy densities not exceeding the boiling limit of the surface layer. Since in the case of boiling an additional source of mass loss is added.

CONCLUSIONS

It has been shown numerically and experimentally that treatment of eutectic silumin with compression plasma flows with an absorbed energy density of 10-35 J/cm^2 leads to melting of the near-surface layer. The maximum thickness of the modified layer after crystallization (45 μm) is achieved at Q=35 J/cm^2. The action of plasma pulses is accompanied by removal of the silumin mass from the surface of the processed material. It has been established that the main mechanism of erosion is the hydrodynamic flow of the melt caused by the expansion of the shock-compressed layer at the surface of the sample during CPF action. Such hydrodynamic flow of the melt to sample edge resulted in melted matter ejection outside the sample. A model based on the assessment of the melt velocity, its maximum temperature and existence time is proposed to estimate the mass removed during plasma impact. The proposed description of surface erosion can be used at absorbed energy densities not exceeding the boiling limit of the surface layer. Good agreement between the experimental and

`

calculated data of the removed mass was find by additionally taking into account the substance remained at the lateral side of the sample as a result of surface tension forces action.

CONFLICT OF INTEREST

1. The authors declare that they have no conflicts of interest.

`

REFERENCES

1. V. S. Zolotorevsky, N. A. Belov, M. V. Glazoff, *Casting Aluminium Alloys* (Elsevier Ltd., Amsterdam, 2007).

2. K. A. Jayasheel Kumar, C. M. Ramesha, M. K. Srinath, B. Navaneeth. Materials Today: Proceedings **59** (1), 483 (2022). https://doi.org/10.1016/j.matpr.2021.11.470

3. V. K. Afanas`eva. *Porshnevye siluminy* (Poligraf, Kemerovo, 2005) (in Russin).

4. K. K. Knipling, D. C. Dunand, D. N. Seidman. Materials Science **97**(3), 246 (2006). https://doi.org/10.1515/ijmr-2006-0042

5. S. Ma, Y. Wang, X. Wang. Journal of Alloys and Compounds **792**, 365 (2019). https://doi.org/10.1016/j.jallcom.2019.04.064

6. L. Bolzoni, M. Nowak, N. Hari Babu Materials and Design **66,** 376 (2015). http://dx.doi.org/10.1016/j.matdes.2014.08.067

7. Dheepa Srinivasan, K. Chattopadhyay. Materials Science and Engineering: A. **304–306,** 534 (2001). https://doi.org/10.1016/S0921-5093(00)01510-0

8. D. V. Zaguliaev, A.A. Klopotov, Y.F. Ivanov, A. M. Ustinov, Y. A. Abzaev and A. D. Teresov. Journal of Physics: Conference Series. **2064**, 012081 (2021). doi:10.1088/1742-6596/2064/1/012081

9. C. M. Abreu, M. J. Cristóbal, R. Figueroa, X. R. Nóvoa, G. Pena. Nuclear Inst. and Methods in Physics Research: B. **442**, 1 (2019). https://doi.org/10.1016/j.nimb.2019.01.013

10. N. N. Cherenda, N. V. Bibik, V. M. Astashynski, A. M. Kuzmitski. High Temperature Material Processes **26**(2), 91 (2022). DOI: 10.1615/HighTempMatProc.2022043681.

11. V. I. Shymanski, A. Jevdokimovs, V. V. Uglov, N. N. Cherenda, V. M. Astashynski, A. M. Kuzmitsky, N. V. Bibik, E. A. Petrikova. Inorg. Mater. Appl. Res. **13** (3), 701 (2022). DOI: 10.1134/S2075113322030340.

12. N. N. Cherenda, N. V. Bibik, V. M. Astashynski, A. M. Kuzmitski. Inorg. Mater. Appl. Res. **15**, 626, (2024). DOI: 10.1134/S2075113324700059

13. J. Puriĉ, I.P. Dojĉinoviĉ, V.M. Astashynski, M.M. Kuraica. Publ. Astron. Obs. Belgrade. **76**, 85 (2003).

14. V. I. Shymanski, A. Jevdokimovs, N. N. Cherenda, V. M. Astashynski, E. A. Petrikova. Journal of the Belarusian State University. Physics. **2**, 25 (2021). DOI: 10.33581/2520-2243-2021-2-25-33.

15. N. N. Cherenda, A. P. Laskovnev, A. V. Basalai, V. V. Uglov, V. M. Astashynski, A. M. Kuzmitski. Inorg. Mater. Appl. Res. **6**, 114 (2015). https://doi.org/10.1134/S2075113315020070.

16. G. A. Bleykher, V. P. Krivobokov. *Foundations of Treatment of Materials by Pulse Electron and Ion Beams* (Tomsk: Publishing House of TPU, 2006).

17. A. A. Kovalev, S. P. Zhvavyi, G. L. Zykov Fizika i texnika poluprovodnikov, **39(11),** 1345 (2005), (in Russian).

18. A. Ya. Leyvi, N. N. Cherenda, V. V. Uglov, A. P. Yalovets. Resource-Efficient Technologies. **3**, 222 (2017). https://doi.org/10.1016/j.reffit.2017.06.003

19. L. D. Landau and V. M. Lifshitz, *Hydrodynamics*. (Science Press, Moscow, 1988).

20. A. N. Babichev, *Fizicheskie velichiny`: Spravochnik* ( M.: E`nergoatomizdat, 1991). (in Russian)

`

TABLES

Table. Depth of the melted layer at different value of Q

The density of the absorbed heat flux energy, J/cm^2	17.0	21.5	27.5	30.0	32.5	35.0
Experimental thickness of the molten layer, μm	20	37	44	32	40	45
Calculated thickness of the molten layer, μm	22	35	50	55	60	65

FIGURE CAPTIONS

Fig. 1. Change in temperature over time on the surface (a) and over the depth of the near-surface layer (b) of eutectic silumin after CPF impact with an absorbed energy density 10 - 55 J/cm^2 (the curves in the figure are presented with a step of 5 J/cm^2).

Fig. 2. SEM images of the silumin samples cross-section after plasma impact with different Q: 10 J/cm^2 (a), 26 J/cm^2 (b), 35 J/cm^2 (c).

Fig. 3. Schematic representations of the shock-compressed layer expansion above the surface of the molten layer (a) and the distribution of melt velocities over the depth of the sample (b).

Fig. 4. SEM image of the sample surface treated with Q=35 J/cm^2.

Fig. 5 Schematic representations of a surface area carried away by melt movement.

Fig. 6 Dependence of mass loss on the density of energy absorbed by the surface layer.

Fig. 7 View of the sample after CPF impact with Q=30 J/cm^2.

`

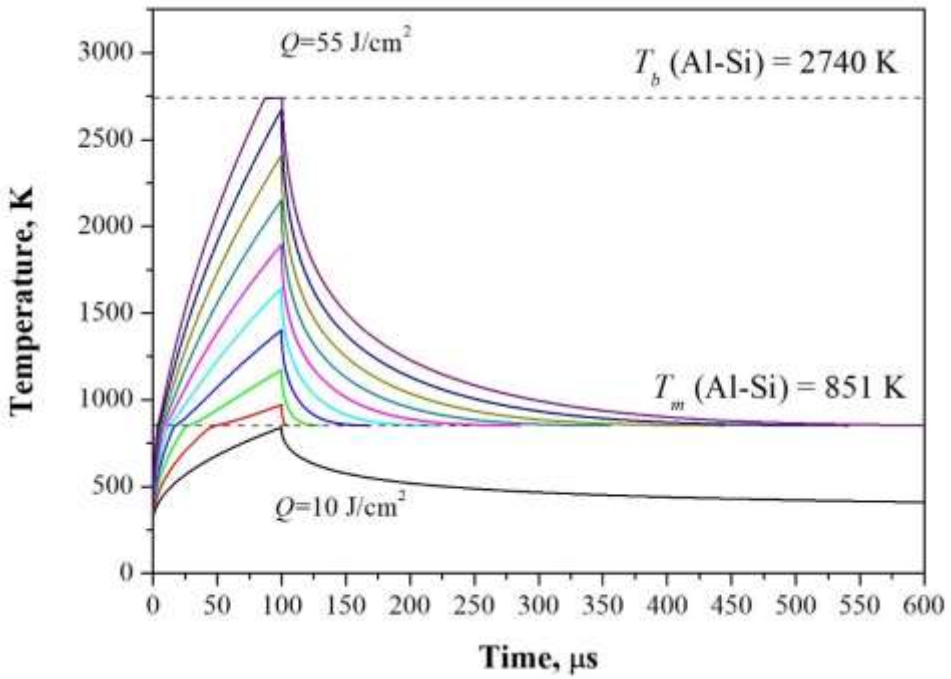
Q=55 J/cm²
T_b (Al-Si) = 2740 K
T_m (Al-Si) = 851 K
Q=10 J/cm²
Temperature, K
Time, μs
0
500
1000
1500
2000
2500
3000
0
50
100
150
200
250
300
350
400
450
500
550
600

a)

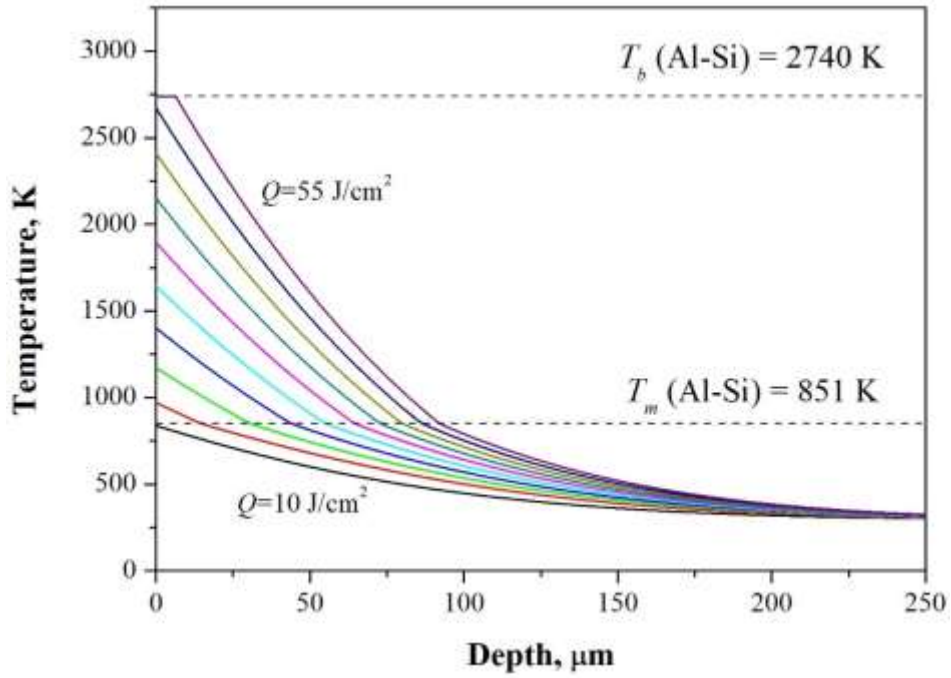
T_b (Al-Si) = 2740 K
Q=55 J/cm²
T_m (Al-Si) = 851 K
Q=10 J/cm²
Temperature, K
Depth, μm
0
500
1000
1500
2000
2500
3000
0
50
100
150
200
250

b)

Fig. 1.

`

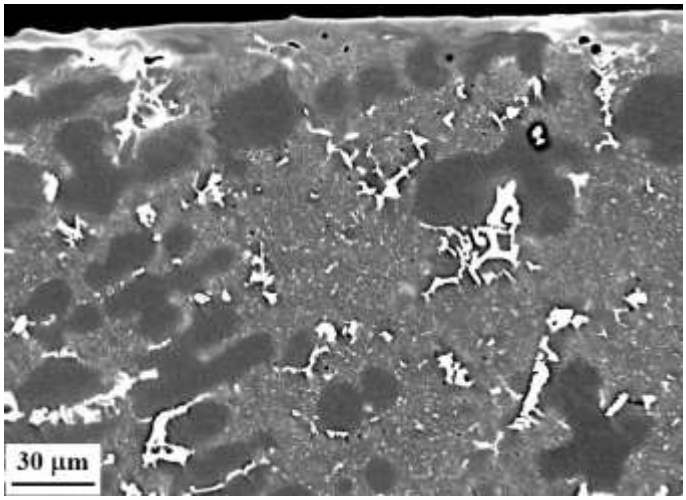

a)

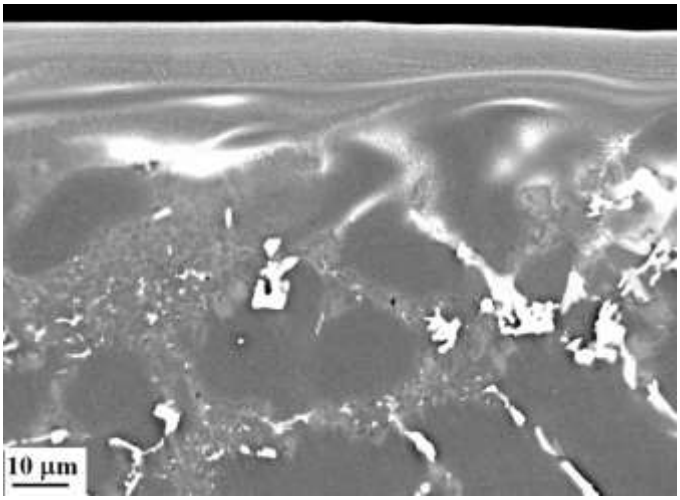

b)

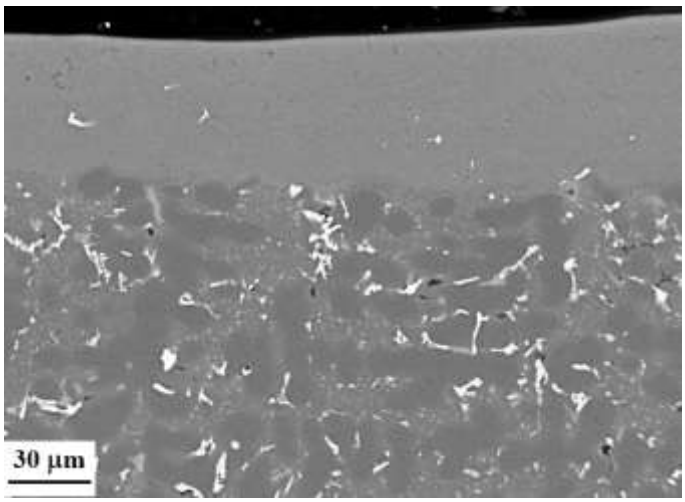

c)

Fig. 2.

`

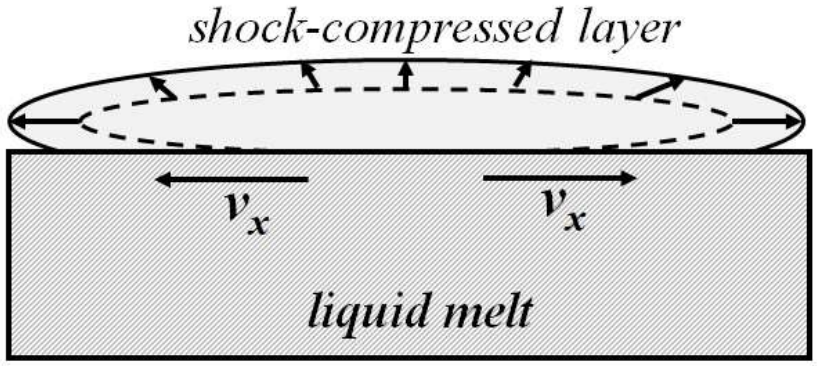

a)

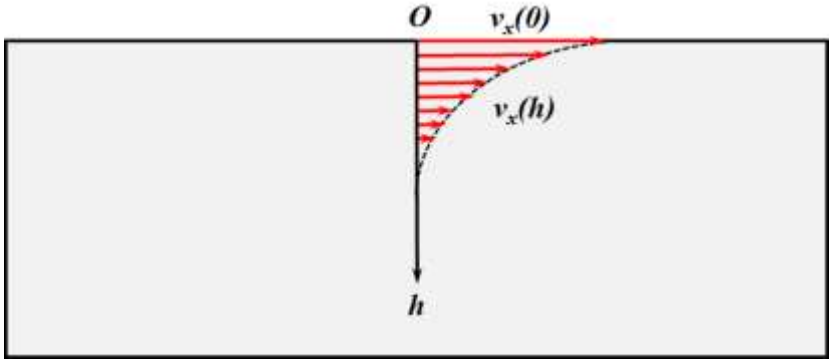

b)

Fig. 3.

`

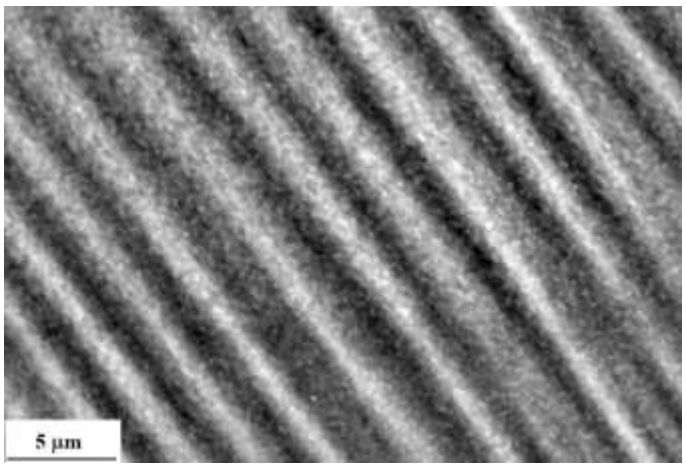

Fig. 4.

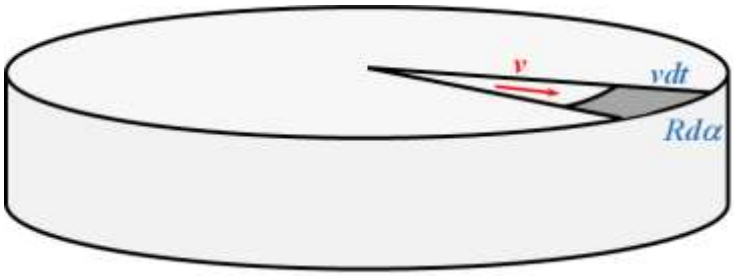

Fig**. 5**

`

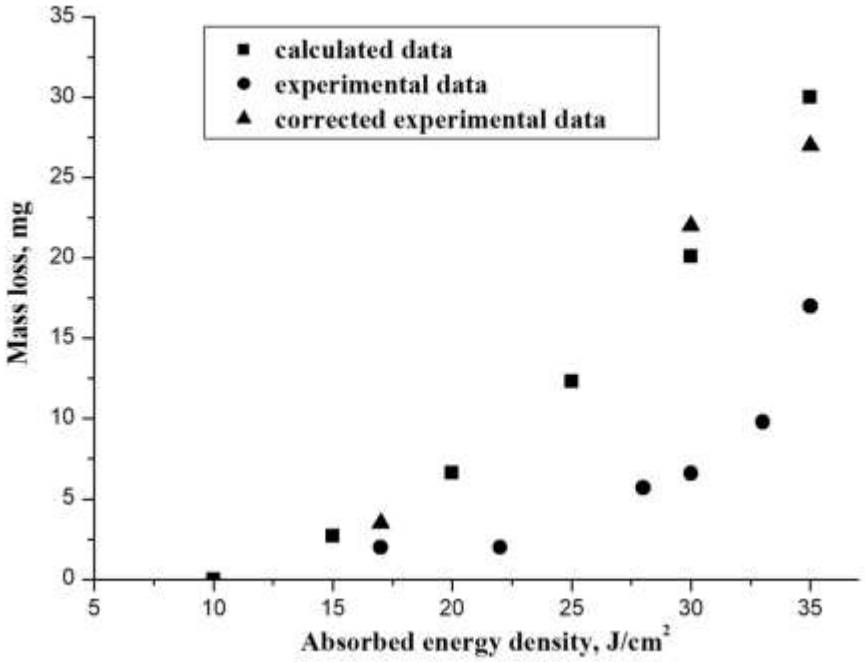
calculated data
experimental data
corrected experimental data
Mass loss, mg
Absorbed energy density, J/cm²
0
5
10
15
20
25
30
35

Fig. 6

Fig. **7**